

Tim Holland · Roger Powell

Activity–composition relations for phases in petrological calculations: an asymmetric multicomponent formulation

Received: 15 June 2002 / Accepted: 4 March 2003 / Published online: 14 May 2003
© Springer-Verlag 2003

Abstract For petrological calculations, including geothermobarometry and the calculation of phase diagrams (for example, P – T petrogenetic grids and pseudosections), it is necessary to be able to express the activity–composition (a – x) relations of minerals, melt and fluid in multicomponent systems. Although the symmetric formalism—a macroscopic regular model approach to a – x relations—is an easy-to-formulate, general way of doing this, the energetic relationships are a symmetric function of composition. We allow asymmetric energetics to be accommodated via a simple extension to the symmetric formalism which turns it into a macroscopic van Laar formulation. We term this the asymmetric formalism (ASF). In the symmetric formalism, the a – x relations are specified by an interaction energy for each of the constituent binaries amongst the independent set of end members used to represent the phase. In the asymmetric formalism, there is additionally a “size parameter” for each of the end members in the independent set, with size parameter differences between end members accounting for asymmetry. In the case of fluid mixtures, for example, H_2O – CO_2 , the volumes of the end members as a function of pressure and temperature serve as the size parameters, providing an excellent fit to the a – x relations. In the case of minerals and silicate liquid, the size parameters are empirical parameters to be determined along with the interaction energies as part of the calibration of the a – x relations. In this way, we determine the a – x relations for feldspars in the systems $KAlSi_3O_8$ – $NaAlSi_3O_8$ and $KAlSi_3O_8$ – $NaAlSi_3O_8$ – $CaAl_2Si_2O_8$, for carbonates in the system $CaCO_3$ – $MgCO_3$, for melt in the melting relationships involving

forsterite, protoenstatite and cristobalite in the system Mg_2SiO_4 – SiO_2 , as well as for fluids in the system H_2O – CO_2 . In each case the a – x relations allow the corresponding, experimentally determined phase diagrams to be reproduced faithfully. The asymmetric formalism provides a powerful and flexible way of handling a – x relations of complex phases in multicomponent systems for petrological calculations.

Introduction

In petrological mineral equilibria calculations, it is necessary to formulate the activity–composition (a – x) relations of multicomponent phases (minerals, fluids and melt). For example, calculation of the PT grid and pseudosections in the system Na_2O – CaO – K_2O – FeO – MgO – Al_2O_3 – SiO_2 – H_2O in White et al. (2001) involves phases which are solutions amongst three end members (alkali feldspars, plagioclase, garnet), four end members (orthopyroxene, biotite), and eight end members (silicate melt). In this context, the regular solution model and its expression as the symmetric formalism (SF, e.g. Powell and Holland 1993) has proved to be a powerful tool in representing the thermodynamics of phases. The main advantages of the SF are (1) that a – x relations of multicomponent phases may be derived from a knowledge of the constituent binary joins without recourse to ternary contributions, and (2) that the models are macroscopic, and so avoid the problems associated with formulating the many pair-wise microscopic (atomistic) interactions in complex multisite phases.

The principal disadvantage of the SF is that it is a symmetric model, and therefore cannot deal accurately with asymmetric mixtures, as reflected in such features as solvi which are skewed towards one end of a binary system. For many practical purposes, regions of a real asymmetric solid solution can be treated as a fictive symmetric solution; however, particularly in phase diagram calculations, a proper asymmetric solution model

T. Holland (✉)
Department of Earth Sciences,
University of Cambridge, Cambridge, CB2 3EQ, UK
E-mail: tjbh@esc.cam.ac.uk

R. Powell
School of Earth Sciences,
University of Melbourne, 3010 Victoria, Australia
Editorial responsibility: B. Collins

has become a necessity. An older model from the literature which has fallen into disuse, the van Laar model, is resuscitated and reformulated in this paper into a convenient form for multicomponent asymmetric solutions. It has both the advantages mentioned above for the symmetric formalism as well as bringing a considerable degree of flexibility to dealing with real asymmetric solutions. Although the van Laar model has been used in the geological literature before (e.g. Powell 1974, 1978; Saxena and Fei 1988; Shi and Saxena 1992; Aranovich and Newton 1999), it has not found favour as a general asymmetric model for solid solutions. Our reformulation of the van Laar model, coined the asymmetric formalism (ASF), allows it to be used in a straightforward and powerful way. This reformulation is outlined, then applied to the representation of the thermodynamics of K–Na–Ca feldspars, CaCO₃–MgCO₃ carbonates, H₂O–CO₂ mixtures and silicate melt in the system Mg₂SiO₄–SiO₂.

Activity–composition relations

In the symmetric formalism (SF) of Powell and Holland (1993), a macroscopic regular model for a – x relations, the activity coefficient for an end member l in a phase with n (independent) end members, is given by

$$RT \ln \gamma_\ell = - \sum_{i=1}^{n-1} \sum_{j>1}^n q_i q_j W_{ij} \quad (1)$$

in which $q_i = 1 - p_i$ when $i = l$ and $q_i = -p_i$ when $i \neq l$. The W_{ij} are macroscopic interaction energies. A proportion, p_i , is the macroscopic fraction of i in the phase, for the particular set of end members used to represent the phase. Although $\sum_{k=1}^n p_k = 1$, individual proportions may be negative. For a given phase, the proportions will change, in general, if a different independent set of end members is chosen. For phases with order–disorder, the number of independent end members, n , is the number of independent macroscopic composition variables plus the number of independent order parameters (Holland and Powell 1996a, 1996b).

In the ASF (van Laar) expressions, asymmetry is introduced via a size parameter for each end member, α_i , such that, when the size parameters are different for the end members in a binary, asymmetry is introduced into that binary. The ASF expressions equivalent to Eq. (1) have the same form

$$RT \ln \gamma_\ell = - \sum_{i=1}^{n-1} \sum_{j>1}^n q_i q_j W_{ij}^* \quad (2)$$

but the constituent terms are now a function of α : $q_i = 1 - \phi_i$ when $i = l$, and $q_i = -\phi_i$ when $i \neq l$, with ϕ_i effectively a size parameter-adjusted proportion

$$\phi_i = \frac{p_i \alpha_i}{\sum_{j=1}^n p_j \alpha_j}$$

W_{ij}^* is a size parameter-adjusted interaction energy,

$$W_{ij}^* = W_{ij} \frac{2\alpha_\ell}{\alpha_i + \alpha_j}$$

Clearly, if the α values for all the end members are the same, Eq. (2) reduces to Eq. (1). In addition, the excess Gibbs energy of mixing is given by

$$G_{ex} = \sum_{i=1}^{n-1} \sum_{j>i}^n \phi_i \phi_j B_{ij}$$

where

$$B_{ij} = \frac{2 \sum_{l=1}^n \alpha_l p_l}{\alpha_i + \alpha_j} W_{ij}$$

The eponymous precursor of the ASF is van Laar (1906) in which asymmetry in mixing relations was introduced via the van der Waals equation. In, for example, Prausnitz et al. (1986), the van der Waals constants were replaced by molar volumes. In the latter's formulation of the van Laar model for a 1–2 binary, the activity coefficient of end member 1 is

$$RT \ln \gamma_1 = V_1 A_{12} \phi_2 (1 - \phi_1) \quad (3)$$

Substituting $A_{12} = \frac{2W_{12}}{V_1 + V_2}$, this reduces to the activity coefficient expression derived from Eq. (2) for a binary. In relation to the form given for the van Laar model in Powell (1974, 1978), the A_1 term therein is equivalent to $\frac{2V_1 W_{12}}{V_1 + V_2}$, and A_2 to $\frac{2V_2 W_{12}}{V_1 + V_2}$. The advantage of the reformulation of the van Laar model in Eq. (2), in contrast to that in Prausnitz et al. (1986) and Powell (1974, 1978), lies in its ease of extension to multicomponent phases, and its clear separation of the interaction energy and size parameter terms.

As an example, to bring out some features of the SF and its extension, the ASF, the activity coefficient of orthoclase (*or*) in ternary feldspar is presented. In the SF it is

$$RT \ln \gamma_{or} = (1 - p_{or}) p_{ab} W_{orab} + (1 - p_{or}) p_{an} W_{oran} - p_{ab} p_{an} W_{aban}$$

One of the essential features of the SF model is that all symmetric microscopic interactions, both from within-site terms and from cross-site terms, always result in a single symmetric macroscopic interaction for any chosen binary (Powell and Holland 1993). In this case, for mixing of K, Na and Ca on the A site, and mixing of Al and Si on two T sites,

$$\begin{aligned} W_{abor} &= W_{NaK}^A \\ W_{aban} &= W_{NaCa}^A + \frac{1}{4} W_{AlSi}^T + \frac{1}{2} W_{CaAlNaSi}^{A-T} \\ W_{oran} &= W_{KCa}^A + \frac{1}{4} W_{AlSi}^T + \frac{1}{2} W_{CaAlKSi}^{A-T} \end{aligned}$$

This points to a problem with microscopic models used for activity modelling, as in the case of W_{aban} , that individual terms are not accessible experimentally. So, for example, the charge difference between Ca⁺⁺ and Na⁺ means that no binary involving just this exchange can be investigated. In the macroscopic approach it

remains useful to interpret a part of the overall mixing energy in terms of such microscopic interactions, while recognising that a macroscopic strain energy may make an important, even dominant, contribution.

The activity coefficient of orthoclase (*or*) in the ASF is

$$RT \ln \gamma_{or} = (1 - \phi_{or}) \phi_{ab} \frac{2\alpha_{or}}{\alpha_{or} + \alpha_{ab}} W_{orab} \\ + (1 - \phi_{or}) \phi_{an} \frac{2\alpha_{or}}{\alpha_{or} + \alpha_{an}} W_{oran} \\ - \phi_{ab} \phi_{an} \frac{2\alpha_{or}}{\alpha_{ab} + \alpha_{an}} W_{aban}$$

The above interpretation of the interaction energies for the SF carry over to the macroscopic interaction energies in the ASF with, additionally, such strain energy contributions from mixing cations or groups of cations of differing size or charge controlling the asymmetry. This is often expressed in large differences in molar volume between end members, although this effect may be masked in structures which have sufficiently flexible frameworks that the overall volume differences are relatively unaffected by substituting cations of different size or charge.

The application of the ASF both to fluids (e.g. H₂O–CO₂) and to solid solutions and silicate melt is straightforward. In the case of fluids, the molar volumes at the *PT* of interest may be used for the size parameters, whereas for solids and silicate melt the size parameters are treated as adjustable parameters which reflect some combination of the local size of interacting atoms or groups of atoms and the resulting strain effects on the mineral lattice. Although the equations are written such that one size parameter is assigned to each end member, the number of size parameters in an *n*-component solution is *n*–1 because it is the ratio of the size parameters which matters, and one of the size parameters may be arbitrarily set (say, at unity).

Although it is not possible to write an expression for the critical temperature and composition for a solvus unless the size parameters are equal (when the regular solution model applies and $T_c = \frac{W}{2rR}$ at $x=0.5$ for a solution with site multiplicity of *n*), the relationships can be shown graphically, as in Fig. 1. As the asymmetry increases, the critical temperature rises slightly, and the critical composition of the solvus top is nearly linearly related to the ratio of the size parameters. Thus, for moderately asymmetrical solvi, a value of *W* may be approximately estimated from the regular solution expression, and the ratio of the size parameters found from the composition of the solvus crest.

The shapes of solvi calculated with the ASF are given in Fig. 2. The solvi become more asymmetric as the parameter $v_2 = \frac{\alpha_2}{\alpha_1 + \alpha_2}$ changes from 0.5 (symmetric) to 0.2 (Fig. 2a). In Fig. 2b, solvi with $v_2=0.6$ at the critical temperature, but with varying temperature-dependence for v_2 , are drawn to show the wide variety of solvus shapes which can be accommodated using the van Laar model. Even more variability may be introduced by making *W* a function of temperature as well.

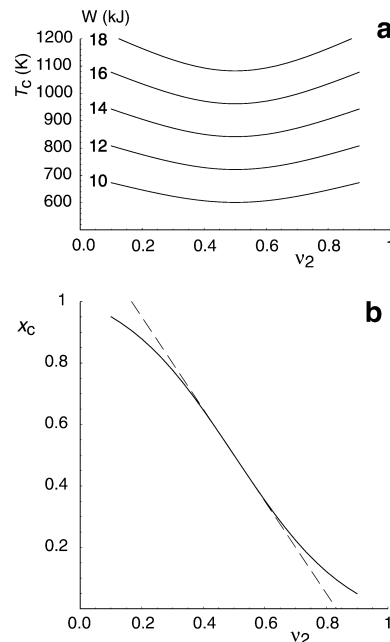


Fig. 1a, b Solvus systematics for the van Laar model. **a** The solvus critical temperature for various values of *W* as a function of the asymmetry parameter $v_2 = \frac{\alpha_2}{\alpha_1 + \alpha_2}$. The solvus crest temperature rises only slightly for moderately asymmetric solvi. **b** The solvus critical composition is close to being linear in the asymmetry parameter v_2

In the petrological literature the subregular model has been much favoured (following Thompson and Waldbaum 1968a, 1968b) as a vehicle for representing asymmetry in solid solutions. This has been a convenient device for binary systems but becomes rather cumbersome when extended to ternary and higher-order solutions. In comparison to the subregular model, the number of overall parameters required in the ASF becomes significantly fewer as *n*, the number of independent end members in the phase, increases. The subregular model may also need extra higher-order terms which are not properties of the constituent individual binary solutions, these being a logical outcome of the third-order polynomial formulation of G_{ex} . The ASF, by contrast, is essentially a quadratic (second-order) model and does not include such ternary terms. This property of building up a complex model solely from its binary properties is a particularly attractive and useful aspect of the ASF model in multicomponent solutions.

Examples

Alkali (and ternary) feldspars

The first example involves the binary KAlSi₃O₈–NaAlSi₃O₈ (sanidine–high albite) alkali feldspar join in which an asymmetric solvus has been experimentally determined. Although both albite and K-feldspar undergo Al–Si ordering, first onto two tetrahedral sites

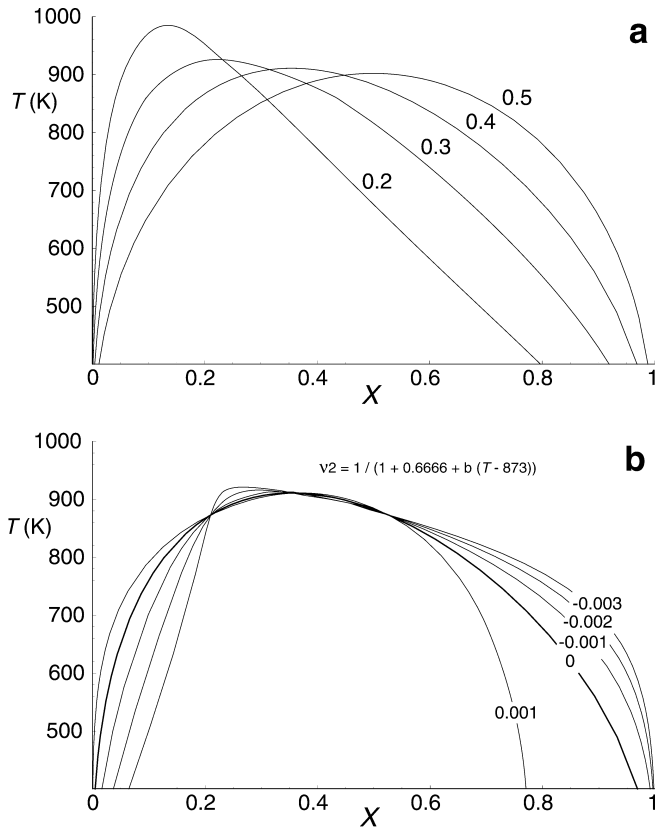


Fig. 2a, b Solvus shapes calculated using the van Laar model. **a** Varying the asymmetry parameter $v_2 = \frac{\alpha_2}{\alpha_1 + \alpha_2}$ for constant W , and **b** varying the temperature-dependence of v_2 for constant W and a value for $v_2 = 0.6$ at the critical temperature

and, with further ordering, of Al onto a single favoured site at low temperatures, the effects of ordering on the solvus will not be taken into account here, the focus being on the high-temperature sanidine–albite solvus. Thompson and Waldbaum (1969) used the experimental data of Bowen and Tuttle (1950), Orville (1963) and Luth and Tuttle (1966) to construct a third-order Margules model (i.e. the subregular model) for the alkali feldspar solvus, and were able to reproduce the experimental data up to 10 kbar. Later experiments at high pressures (from 9 to 15 kbar) were performed by Goldsmith and Newton (1974) who found that the Thompson and Waldbaum model extrapolated remarkably well to the conditions of their experiments. We now (1) demonstrate that the ASF described above can reproduce the experimental data faithfully, and (2) use the binary model as a platform for the construction of a ternary feldspar solution model involving the additional anorthite component.

The model parameters to be fitted to the experiments are the size parameters for the albite and sanidine end members (α_{ab} and α_{san}) and the interaction energy W_{absan} for the binary. Because it is only the ratio of the two size parameters which determines the thermodynamics, one is set at unity (here α_{san} is chosen), leaving the other as

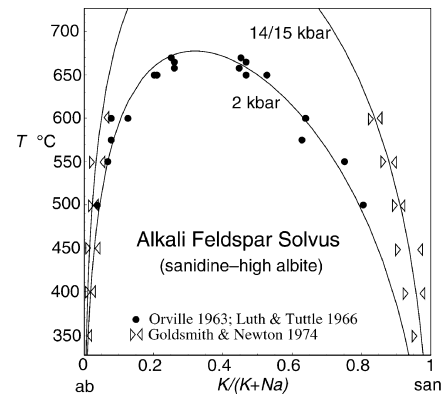


Fig. 3 Calculated solvus for sanidine–high-albite feldspars. The 2-kbar data are those selected by Thompson and Waldbaum (1969) for their analysis. The brackets from Goldsmith and Newton at 14 and 15 kbar are combined here, and the curve is that calculated for 14.5 kbar (calculated using THERMOCALC; Powell and Holland 1988; Powell et al. 1998)

the adjustable parameter. The two equilibrium equations relating compositions of coexisting feldspars are

- 1) KAlSi_3O_8 (albite) = KAlSi_3O_8 (sanidine) and
- 2) $\text{NaAlSi}_3\text{O}_8$ (albite) = $\text{NaAlSi}_3\text{O}_8$ (sanidine),

so the activity of the sanidine end member must be the same in both phases coexisting across the solvus (and likewise for the albite end member). By equating $RT \ln X_i \gamma_i$ for each end member at each temperature for coexisting pairs, and taking experimental values for the X_i , the values for the unknown parameters may be found by non-linear regression, using the following equations for the activity coefficients

$$RT \ln \gamma_{san} = \frac{2\alpha_{san}}{\alpha_{san} + \alpha_{ab}} \phi_{ab}^2 W_{absan} \quad (4)$$

$$RT \ln \gamma_{ab} = \frac{2\alpha_{ab}}{\alpha_{san} + \alpha_{ab}} \phi_{san}^2 W_{absan} \quad (5)$$

We have used the experimental points selected by Thompson and Waldbaum (1969) in their original analysis, supplemented by several reversals between 9 and 15 kbar from Goldsmith and Newton (1974). Figure 3 shows the calculated solvi at 2 and 14.5 kbar, together with the experimental data. The model fits the experimental data well, using just four adjustable parameters, as follows (with T in K and P in kbar):

$$W_{absan} = 25.1(\pm 2.0) - 0.0108(\pm 0.0022)T \\ + 0.343(\pm 0.025)PkJ, \text{ and } \alpha_{ab} = 0.643(\pm 0.018),$$

with α_{san} set at 1.0.

The size parameters for sanidine (1.0) and albite (0.643) are more disparate than would be suggested from the molar volumes of these end members (10.9 and 10.1 J bar⁻¹ respectively) but are much closer to the relative ionic radii of K⁺ and Na⁺ (1.33 vs. 0.97). Presumably the size parameters are governed in part by factors which include the cation size mismatch and by

the resulting local strain effects in the feldspar structure, whereas the molar volume differences between albite and sanidine are moderated by the flexibility of the Al–Si framework.

The KAlSi_3O_8 – $\text{NaAlSi}_3\text{O}_8$ solvus serves as a starting point in calibrating the coexisting plagioclase and alkali feldspar in the ternary feldspar system KAlSi_3O_8 – $\text{NaAlSi}_3\text{O}_8$ – $\text{CaAl}_2\text{Si}_2\text{O}_8$. This system has been investigated extensively by Ghiorso (1984), Green and Usdansky (1986), Fuhrmann and Lindsley (1988) and Elkins and Grove (1990), using the Margules formulation for mixing energetics. Elkins and Grove (1990) analysed their experimental results in the range 700–900 °C, with a one-site entropy of mixing and a subregular solution. The tie lines between calcic plagioclase and alkali feldspars show a clear change in slope relative to the tie lines between sodic plagioclase and alkali feldspars, this change occurring around the an_{50} composition. We have reinvestigated the system, using the Elkins and Grove experimental data, separating the plagioclase feldspars into an albite-rich $C1$ solid solution and an anorthite-rich $I1$ solid solution, using the Darken's quadratic formalism (DQF, Powell 1987) approach used by Holland and Powell (1992). Plagioclase compositions more anorthite-rich than given by the $C1$ – $I1$ boundary, $X_{an}^b = 0.12 + 0.00038 T(\text{K})$ (Carpenter and McConnell 1984) are taken as belonging to the $I1$ solid solution.

Three internal equilibria were used, one for each of the three feldspar end members, to determine the parameters for mixing in the anorthite–albite–sanidine system. The model discussed above was used for the albite–sanidine binary. The standard state used is the Gibbs energy of the pure end members in their stable structural state, i.e. $C1$ for albite and sanidine, and $I1$ for anorthite. Thus, for the $C1$ solid solutions, a Gibbs energy increment (the DQF parameter I_{an}) is required to convert the anorthite Gibbs energies to that of a fictive anorthite with the $C1$ structure. Similarly, a Gibbs energy increment for albite in the $I1$ structure feldspar is required. The model was fitted to the coexisting plagioclase and alkali feldspars from the experimental dataset of Elkins and Grove (1990) in two stages. Firstly, the $C1$ coexisting feldspars (i.e. the pairs involving plagioclase with less than 50% anorthite content) were regressed to give the values for the additional parameters W_{ansan}^{C1} , W_{anab}^{C1} , and α_{an}^{C1} . The resulting fits to the data are shown in Fig. 4 where the slopes of the tie lines and calculated compositions agree well with the original experimental data. The parameter values from the regression are

$$\begin{aligned} W_{ansan}^{C1} &= 40 (\pm 1.5) \text{ kJ} \\ W_{anab}^{C1} &= 3.1 (\pm 1.3) \text{ kJ} \\ \alpha_{an}^{C1} &= 1.0 (\pm 0.15). \end{aligned} \quad (6)$$

The second stage involves fitting to the pairs of feldspars involving $I1$ plagioclase, of which there are only three experimental brackets, all at 900 °C. With so few brackets, it was decided to keep the values for W_{ansan}^{I1} and α_{an}^{I1} the same as for the $C1$ solutions, and solve for

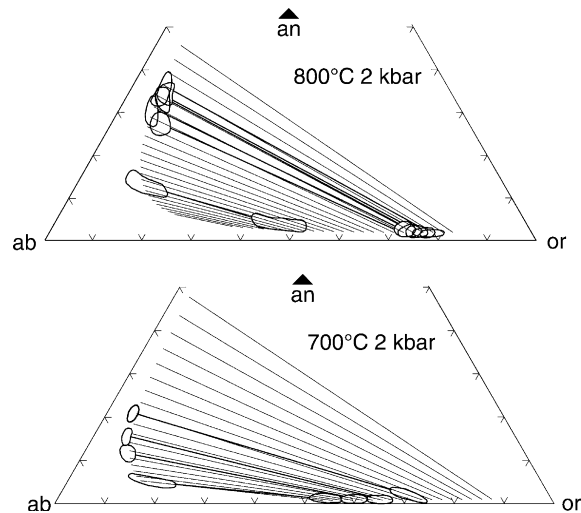


Fig. 4 Calculated $C1$ ternary feldspar compositions (tie lines) and experimental data (fields) at (above) 800 °C and 2 kbar, (below) 700 °C and 2 kbar. The experimental pair at low X_{an} at 800 °C is at 1 kbar. Thick tie lines and experimental data fields are taken from Elkins and Grove (1990; calculated using THERMOCALC)

the value of W_{anab}^{I1} . The values for the DQF parameters I_{an} and I_{ab} are constrained from the position of the $C1$ – $I1$ transition in plagioclase feldspars, as determined by Carpenter and McConnell (1984) as follows: for $C1$ plagioclase,

$$\begin{aligned} RT \ln \gamma_{ab} &= \frac{2\alpha_{ab}}{\alpha_{an} + \alpha_{ab}} \phi_{an}^2 W_{aban}^{C1} \\ RT \ln \gamma_{an} &= \frac{2\alpha_{an}}{\alpha_{an} + \alpha_{ab}} \phi_{ab}^2 W_{aban}^{C1} + I_{an} \end{aligned} \quad (7)$$

and for $I1$ plagioclase,

$$\begin{aligned} RT \ln \gamma_{ab} &= \frac{2\alpha_{ab}}{\alpha_{an} + \alpha_{ab}} \phi_{an}^2 W_{aban}^{I1} + I_{ab} \\ RT \ln \gamma_{an} &= \frac{2\alpha_{an}}{\alpha_{an} + \alpha_{ab}} \phi_{ab}^2 W_{aban}^{I1} \end{aligned} \quad (8)$$

Equating the values of $RT \ln \gamma$ at the composition of the phase boundary $X_{an} = X_{an}^b$ gives expressions for I_{ab} and I_{an}

$$\begin{aligned} I_{ab} &= -2 \frac{2\alpha_{ab}}{\alpha_{ab} + \alpha_{an}} \phi_{an}^2 \Delta W \\ I_{an} &= 2 \frac{2\alpha_{an}}{\alpha_{ab} + \alpha_{an}} \phi_{ab}^2 \Delta W \end{aligned} \quad (9)$$

where $\Delta W = W_{aban}^{I1} - W_{aban}^{C1}$. Knowing the value for X_{an}^b at 900 °C (0.57) from Carpenter and McConnell (1984), once the two W parameters are known, the two I parameters may be calculated as a function of temperature for the $C1$ – $I1$ boundary, giving the additional model parameters used to generate Fig. 5:

$$\begin{aligned} W_{ansan}^{I1} &= 40 (\pm 1.5) \text{ kJ} \\ W_{anab}^{I1} &= 15 (\pm 3) \text{ kJ} \\ \alpha_{an}^{I1} &= 1.0 (\pm 0.15) \\ I_{an} &= 7.03 - 0.00466T (\pm 0.2) \text{ kJ} \\ I_{ab} &= 0.57 - 0.00412T (\pm 0.2) \text{ kJ} \end{aligned} \quad (10)$$

The tie-line slopes for calcic plagioclase–orthoclase pairs in Fig. 5 do not match the experimental data

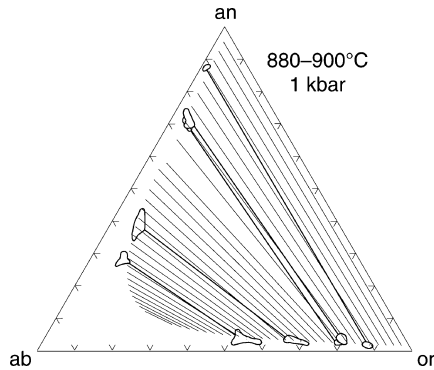


Fig. 5 Calculated ternary feldspar compositions (*tie lines*) and experimental data (*fields*) at 900 °C and 1 kbar. Plagioclase at $X_{an} > 0.6$ is assumed to be *I1* structure. *Thick tie lines* and experimental *data fields* are taken from Elkins and Grove (1990; calculated using THERMOCALC)

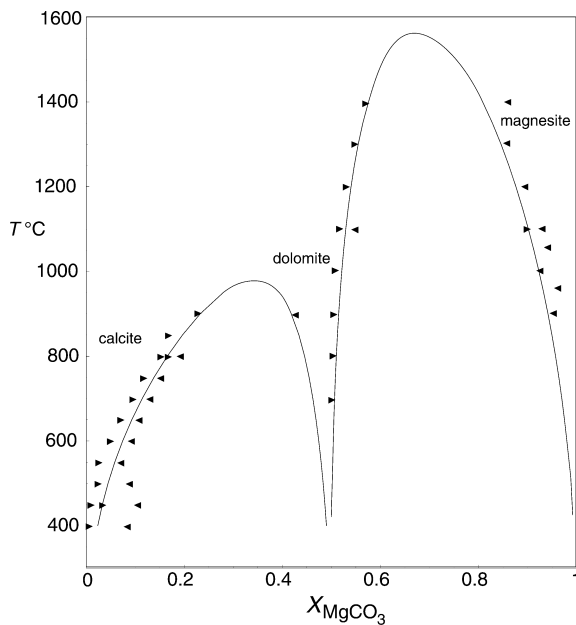


Fig. 6 Calculated solvi in the calcite–dolomite–magnesite system. Experimental brackets are taken from Anovitz and Essene (1987; calculated using THERMOCALC)

perfectly. This may be in part due to the simplifications introduced here (taking a one-site entropy of mixing model, a simplified DQF plagioclase model, and the assumption that W_{ansan} is the same in *C1* and *I1* feldspars). Nevertheless, the model works remarkably well overall and, in addition, produces activity–composition relations for plagioclase feldspars which are very similar to those in Holland and Powell (1992).

Calcite–dolomite–magnesite

The Ca–Mg carbonates exhibit both exsolution and order–disorder behaviour, with strong Ca–Mg ordering at the dolomite composition leading to a pair of solvi

which are both asymmetric and of unequal critical temperature (Fig. 6). Experimental studies, such as the one of Goldsmith and Newton (1969), form the basis of the diagram which is taken from the summary of Anovitz and Essene (1987). These features of the carbonate system calcite–dolomite–magnesite pose a particularly difficult challenge to thermodynamic modelling. It is important to develop a model which is continuous between magnesite and calcite, and which is capable of generating an ordered dolomite field, rather than treating calcite–dolomite and dolomite–magnesite as two separate solid solutions. The model discussed below involves a non-ideal calcite–magnesite solution which would lead to a wide solvus in the absence of ordering. By using an order–disorder model similar to that used for omphacite (Holland and Powell 1996b), it is possible to generate a field of ordered dolomite between a pair of miscibility gaps which separate it from disordered calcite and magnesite. The model is quite simple, and treats this binary join as a fictive ternary between the three two-site end members calcite (*cc*, $\text{Ca}_2(\text{CO}_3)_2$), dolomite (*dol*, $\text{CaMg}(\text{CO}_3)_2$) and magnesite (*mag*, $\text{Mg}_2(\text{CO}_3)_2$). Order–disorder is treated by assigning a free energy (ΔG_R) to the internal equilibrium relation



and by allowing N moles of Ca to move from the $M1$ to the $M2$ site (and of Mg to the $M2$ from the $M1$ site), such that the site fractions become

$$\begin{aligned} x_{Ca}^{M2} &= 1 - X + N \\ x_{Mg}^{M2} &= X - N \\ x_{Ca}^{M1} &= 1 - X - N \\ x_{Mg}^{M1} &= X + N \end{aligned} \quad (11)$$

where the bulk composition X can be written as $X = \frac{1}{2}x_{Mg}^{M1} + \frac{1}{2}x_{Mg}^{M2}$. The proportions (or mole fractions) of the end members are

$$\begin{aligned} p_{cc} &= x_{Ca}^{M1} = 1 - X - N \\ p_{mag} &= x_{Mg}^{M2} = X - N \\ p_{dol} &= x_{Mg}^{M1} - x_{Mg}^{M2} = 2N \end{aligned} \quad (12)$$

The ideal mixing on sites activities (e.g. Wood and Banno 1973; Powell 1978; Anderson and Crerar 1993) are

$$\begin{aligned} a_{cc}^{ideal} &= x_{Ca}^{M2} x_{Ca}^{M1} \\ a_{mag}^{ideal} &= x_{Mg}^{M2} x_{Mg}^{M1} \\ a_{dol}^{ideal} &= x_{Ca}^{M2} x_{Mg}^{M1} \end{aligned}$$

and the ASF activity coefficients (where $c = cc$, $d = dol$, and $m = mag$)

$$\begin{aligned} RT \ln \gamma_c &= (1 - \phi_c) \phi_m W_{cm} \frac{2\alpha_c}{\alpha_c + \alpha_m} + (1 - \phi_c) \phi_d \\ &\times W_{cd} \frac{2\alpha_c}{\alpha_c + \alpha_d} - \phi_m \phi_d W_{md} \frac{2\alpha_c}{\alpha_m + \alpha_d} \end{aligned}$$

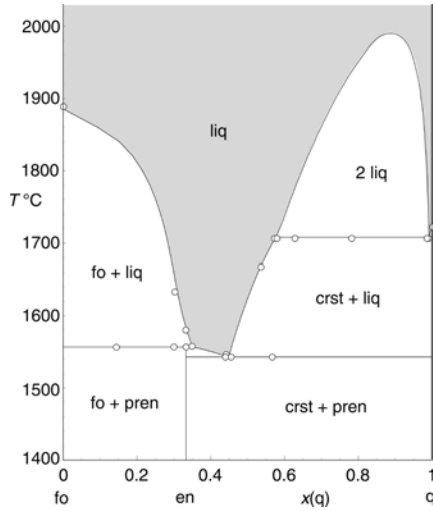


Fig. 7 Calculated phase diagram and experimental data for the forsterite–silica system at atmospheric pressure. The experiments are from Bowen and Anderson (1914) and Greig (1927). The temperatures from Greig (1927) for the univariant horizontal line involving two liquids + cristobalite have been raised to agree with Ol’shanskii (1952; calculated using THERMOCALC)

$$\begin{aligned}
 RT \ln \gamma_m &= (1 - \phi_m) \phi_c W_{cm} \frac{2\alpha_m}{\alpha_c + \alpha_m} - \phi_c \phi_d W_{cd} \frac{2\alpha_m}{\alpha_c + \alpha_d} \\
 &\quad + (1 - \phi_m) \phi_d W_{md} \frac{2\alpha_m}{\alpha_m + \alpha_d} \\
 RT \ln \gamma_d &= -\phi_c \phi_m W_{cm} \frac{2\alpha_d}{\alpha_c + \alpha_m} + (1 - \phi_d) \phi_c W_{cd} \frac{2\alpha_d}{\alpha_c + \alpha_d} \\
 &\quad + (1 - \phi_d) \phi_m W_{md} \frac{2\alpha_d}{\alpha_m + \alpha_d} \quad (13)
 \end{aligned}$$

The parameters used in constructing Fig. 6 are

$$\begin{aligned}
 \Delta G_R &= -13.5 \text{ kJmol}^{-1} \\
 W_{ccmag} &= 70.0 \text{ kJmol}^{-1} & W_{ccdol} &= 20.5 \text{ kJmol}^{-1} \\
 W_{magdol} &= 29.9 \text{ kJmol}^{-1} \\
 \alpha_{mag} &= 1.0 & \alpha_{dol} &= 0.7 & \alpha_{cc} &= 0.50 + 0.000546 T
 \end{aligned}$$

The size parameters are dimensionless and normalised to unit value for magnesite. The degree of asymmetry exhibited by the calcite–dolomite solvus required a temperature-dependence for α_{cc} . The parameters have been chosen for the purposes of illustrating the model, but may be subject to revision when a fuller treatment of the calcite–magnesite–siderite system is attempted. We wish to emphasize that the miscibility gaps are not treated as two separate binary models, but that the single set of parameters listed above generates the complete phase diagram, including the changing state of order in the carbonates. In this respect, the state of order in the dolomite is predicted to be high even at the highest temperatures shown on the diagram.

Forsterite–enstatite–silica melting

Another instance where an asymmetric model is critical is in silicate melting, for example, where unmixing of

two silicate liquids occurs close to the SiO_2 composition in the forsterite–silica (Mg_2SiO_4 – SiO_2) binary system. Symmetric models are inadequate for representing the phase equilibria, and we present an analysis of this system using the ASF model in Fig. 7, where the temperatures and compositions of the univariant equilibria forsterite–protoenstatite–liquid, protoenstatite–cristobalite–liquid, and cristobalite–two liquids are remarkably well reproduced by the model. The compositional binary is approximated by a fictive ternary made up of the end members forsterite liquid (foL , $\text{Mg}_4\text{Si}_2\text{O}_8$), enstatite liquid (enL , $\text{Mg}_{8/3}\text{Si}_{8/3}\text{O}_8$) and silica liquid (qL , SiO_8), all expressed in eight-oxygen units. These units are assumed to mix ideally in terms of the entropy of mixing, but the ASF is used to express the non-ideal enthalpic contribution. In this interpretation of the thermodynamics, the mole proportion of the protoenstatite “molecule” in solution is analogous to an order parameter, taking on values from zero for a disordered solution to unity for a fully ordered solution at the protoenstatite bulk composition.

On an eight-oxygen basis, the enL composition is given by $enL = \frac{2}{3}foL + \frac{1}{3}qL$ and, using the two variables x and y to represent bulk silica and order parameter respectively, the following relations hold:

$$\begin{aligned}
 x &= \frac{qL}{foL + qL} \\
 a_{enL}^{ideal} &= p_{enL} = y \\
 a_{qL}^{ideal} &= p_{qL} = x - \frac{y}{3} \\
 a_{foL}^{ideal} &= p_{foL} = 1 - x - \frac{2y}{3}
 \end{aligned}$$

and the activity coefficients are written using a ternary van Laar expression analogous to that written above (Eq. 13) for the calcite–dolomite–magnesite system in which the ϕ values are calculated using the end-member proportions as derived above. The Gibbs free energy of the internal equilibrium reaction

$$enL = \frac{2}{3}foL + \frac{1}{3}qL$$

is taken directly from the thermodynamic data in Holland and Powell (1998), and the values for the three interaction energies $W_{foL\ enL}$, $W_{foL\ qL}$ and $W_{qL\ enL}$ as well as the size parameters α_{foL} and α_{qL} (with α_{enL} set at unity) were found by least-squares fitting to the experimental data of Bowen and Anderson (1914) and Greig (1927).

The van Laar parameters used in constructing Fig. 7 are

$$\begin{aligned}
 W_{foL\ qL} &= 40.0 \text{ kJmol}^{-1} & W_{foLenL} &= 21.0 \text{ kJmol}^{-1} \\
 W_{enL\ qL} &= 139.5 - 0.046 T \text{ kJmol}^{-1} \\
 \alpha_{enL} &= 1.0 & \alpha_{foL} &= 0.46 & \alpha_{qL} &= 0.30
 \end{aligned}$$

The temperatures and compositions of the calculated univariant equilibria in Fig. 7 are within ± 2 °C and ± 0.04 respectively of the experimental determinations. The univariant between two liquids and cristobalite is calculated at 1,707 °C, higher than the data of Greig

(1927) but in better agreement with the more recent data of Ol'shanskii (1951).

The success of this model has been made possible by three assumptions about the mixing. Firstly, the use of an order–disorder model involving the enL component acting as a dominant species has allowed the thermodynamics of the foL – qL binary to behave like two nearly decoupled subsystems (foL – enL and enL – qL). Secondly, the use of eight-oxygen units gives some entropic asymmetry to the effective enL – qL sub-binary, and allows the liquid immiscibility gap to move to more silica-rich compositions. Thirdly, the van Laar model allows enough additional asymmetric behaviour to fit the phase diagram features quantitatively.

H₂O–CO₂

Aranovich and Newton (1999) performed experiments to determine the mixing properties for binary H₂O–CO₂ mixtures and used a van Laar expression to fit their results. They showed that, as well as fitting their results extremely well, the resulting activities were in close agreement with the Kerrick and Jacobs (1981) version of the modified Redlich Kwong (MRK) equation of state for these mixtures.

Writing the activity coefficients using the van Laar equations (h =H₂O, c =CO₂), and taking the size parameters to be the molar volumes of the end members at P and T gives

$$RT \ln \gamma_h = 2 \frac{V_h V_c}{V_h + V_c} \frac{V_c}{(p_h V_h + p_c V_c)^2} W_{hc} p_c^2 \quad (14)$$

Aranovich and Newton fitted W_{hc} as a function of pressure and temperature which, although fitting the data over the PT range of their experiments, does not agree well with the MRK predictions at very high pressure. By comparing the value of W_{hc} as obtained by fitting to the MRK equation of state (Kerrick and Jacobs 1981), it is clear that W_{hc} appears to vary nearly linearly with the inverse molar volume of the mixture, in particular the product $W_{hc} \frac{V_h V_c}{V_h + V_c}$ remaining virtually constant over the range 0.5–20 kbar, 400–1,000 °C. Thus, for H₂O–CO₂ mixtures we have $W_{hc} = a_{hc} \frac{V_h + V_c}{V_h V_c}$, with a_{hc} around 12.0 kJ²kbar⁻¹. The van Laar expressions for Gibbs energy and activity coefficients can therefore be simplified considerably to

$$G^{\text{ex}} = \frac{2a_{hc}}{(p_h V_h + p_c V_c)} p_h p_c \quad (15)$$

$$RT \ln \gamma_h = \frac{2a_{hc} V_c}{(p_h V_h + p_c V_c)^2} p_c^2 \quad (16)$$

$$RT \ln \gamma_c = \frac{2a_{hc} V_h}{(p_h V_h + p_c V_c)^2} p_h^2 \quad (17)$$

With this convenient functional form for the PT dependence of the van Laar W parameter, we refitted the

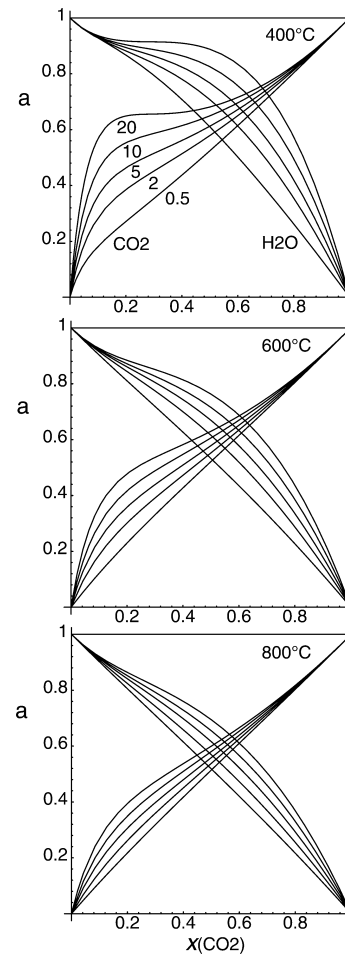


Fig. 8 Activity–composition plots for H₂O–CO₂ at 400, 600 and 800 °C, calculated from the van Laar model discussed in the text. Contours are at 0.5, 2, 5, 10 and 20 kbar

experiments of Aranovich and Newton (1999), along with all the dehydration and decarbonation experiments used in building the dataset of Holland and Powell (1998), to find the optimum value for the van Laar interaction energy parameter given by the phase equilibrium data. The best fit obtained by least squares was $a_{hc} = 10.5 \pm 0.5$ kJ²kbar⁻¹. This value is slightly smaller than that derived from the MRK equation of state (12 kJ²kbar⁻¹), suggesting that the latter slightly overestimates the non-ideality in H₂O–CO₂ mixtures at the higher pressures and temperatures of the experiments. Following the same procedure, using the standard sub-regular model produced a less good fit of the data.

Figure 8 shows the calculated activities in the H₂O–CO₂ system at a variety of pressures and temperatures. They are very similar to, but slightly more ideal than the Kerrick and Jacobs (1981) MRK activities over the range of PT (0.5–20 kbar, 400–1,000 °C). The one-parameter ASF model presented here is only in semi-quantitative agreement with the precise molar volumes and activities determined by Blencoe et al. (1999) at 400 °C. It is probable that the parameter a_{hc} fails to remain constant once pressures and temperatures

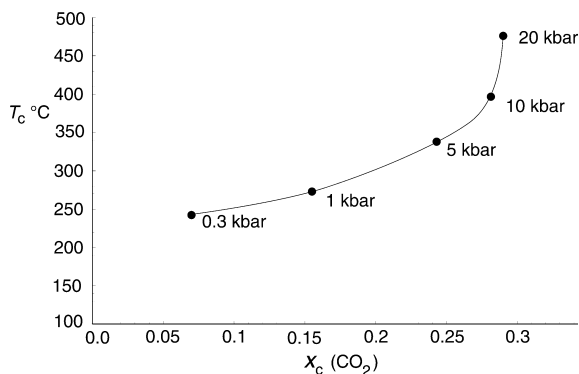


Fig. 9 Unmixing relationships for H₂O–CO₂ as a function of pressure, given as a plot of critical temperature against critical composition

approach those of the critical point of H₂O. This is not surprising, given that Blencoe et al. (1999) needed to use three separate and considerably more complex equations to reproduce their data as a function of pressure for just the 400 °C isotherm. It is, nevertheless, quite remarkable that a single adjustable parameter can fit the H₂O–CO₂ activity data well over such a large *PT* range, covering most of the facies in metamorphic petrological applications. H₂O and CO₂ become immiscible at low temperatures, and Fig. 9 shows the calculated critical temperature and composition for immiscibility in the H₂O–CO₂ binary as a function of pressure, and it suggests that unmixing may be common at conditions within the blueschist and low-temperature eclogite facies. The solvus becomes extremely asymmetric at low pressures where the molar volumes of H₂O and CO₂ diverge markedly. The 1-kbar solvus crest at 273 °C and $X_{\text{CO}_2} = 0.17$ is in good agreement with the experimental determinations of Todheide and Franck (1963) and Takeneuchi and Kennedy (1964).

If the ASF model with constant a_{ij} parameters can represent the H₂O–CO₂ activities well over a large range of *PT* conditions, then it is likely that the approach will be useful in multicomponent fluids in the COH system. When values for van Laar W_{ij} from pairs of gases in the system H₂O–CO₂–CO–CO₂–H₂–CH₄ are determined using the Holloway-Flowers MRK equation of state (Holloway 1977; Flowers 1979), the following a_{ij} parameters (kbar⁻¹) are obtained.

a_{ij}	CO ₂	CH ₄	H ₂	CO
H ₂ O	12.0	15.5	14.9	16.8
CO ₂		0.6	2.2	1.2
CH ₄			0.8	0.0
H ₂				0.3

This table brings out the fact that mixing of H₂O with other species is very non-ideal whereas the other gases mix nearly ideally among themselves, a feature stemming from the polar nature of the H₂O molecule. With the a_{ij} values above, the W_{ij} may be found at any desired *PT* and the activity coefficients determined for complex gas mixtures through Eq. (2).

In summary, the examples above illustrate both the simplicity and the utility of the ASF model in tackling petrological problems with multicomponent solid and fluid solutions, especially where several constituent binary joins are quite asymmetric. The model should find particular application in the development of multicomponent melt models, as well as in increasing the flexibility in accounting for order–disorder in solid solutions by extending the SF approach of Holland and Powell (1996b).

Acknowledgements We thank Frank Spear, James Blencoe and Jamie Connolly for their valuable comments which led to improvement of the manuscript. Any errors remaining are ours.

References

- Anovitz LM, Essene EJ (1987) Phase equilibria in the system CaCO₃–MgCO₃–FeCO₃. *J Petrol* 28:389–414
- Anderson GM, Crerar DA (1993) *Thermodynamics in Geochemistry*. University Press, Oxford
- Aranovich LY, Newton RC (1999) Experimental determination of CO₂–H₂O activity–composition relations at 600–1,000 °C and 6–14 kbar by reversed decarbonation and dehydration reactions. *Am Mineral* 84:1319–1332
- Blencoe JG, Seitz JC, Anovitz LM (1999) The CO₂–H₂O system II. Calculated thermodynamic mixing properties for 400 °C, 0–400 MPa. *Geochim Cosmochim Acta* 63:2393–2408
- Bowen NL, Anderson O (1914) The binary system MgO–SiO₂. *Am J Sci* 37:487–500
- Bowen NL, Tuttle OF (1950) The system NaAlSi₃O₈–KAlSi₃O₈–H₂O. *J Geol* 58:489–511
- Carpenter MA, McConnell JDC (1984) Experimental delineation of the C1–I1 transformation in intermediate plagioclase feldspars. *Am Mineral* 69:112–121
- Elkins LT, Grove TL (1990) Ternary feldspar experiments and thermodynamic models. *Am Mineral* 75:544–559
- Flowers GC (1979) Correction of Holloway's (1977) adaptation of the Modified Redlich-Kwong equation of state for the calculation of the fugacities of molecular species in supercritical fluids of geological interest. *Contrib Mineral Petrol* 69:315–318
- Fuhrman ML, Lindsley DH (1988) Ternary feldspar modeling and thermometry. *Am Mineral* 73:201–215
- Ghiorso MS (1984) Activity/composition relations in the ternary feldspars. *Contrib Mineral Petrol* 87:282–296
- Goldsmith JR, Newton RC (1969) P–T–X relations in the system CaCO₃–MgCO₃ at high temperatures and pressures. *Am J Sci* 267 A:160–190
- Goldsmith JR, Newton RC (1974) An experimental determination of the alkali feldspar solvus. In: MacKenzie WS, Zussman J (eds) *The Feldspars*. University Press, Manchester
- Green NL, Urdansky ST (1986) Ternary feldspar relations and feldspar thermobarometry. *Am Mineral* 71:1100–1108
- Greig JW (1927) Liquid immiscibility in the system FeO–Fe₂O₃–Al₂O₃–SiO₂. *Am J Sci* 14:473–484
- Holland TJB, Powell R (1992) Plagioclase feldspars: activity–composition relations based upon Darken's quadratic formalism and Landau theory. *Am Mineral* 77:53–61
- Holland TJB, Powell R (1996a) Thermodynamics of order–disorder in minerals 1: symmetric formalism applied to minerals of fixed composition. *Am Mineral* 81:1413–1424
- Holland TJB, Powell R (1996b) Thermodynamics of order–disorder in minerals 2: symmetric formalism applied to solid solutions. *Am Mineral* 81:1425–1437
- Holland TJB, Powell R (1998) An internally-consistent thermodynamic data set for phases of petrological interest. *J Metamorph Geol* 16:309–343

- Holloway JR (1977) Fugacity and activity of molecular species in supercritical fluids. In: Fraser DG (ed) *Thermodynamics in geology*. Reidel, Dordrecht, pp 161–181
- Kerrick DM, Jacobs GK (1981) A modified Redlich-Kwong equation for H₂O, CO₂ and H₂O–CO₂ mixtures at elevated pressures and temperatures. *Am J Sci* 281:735–767
- Luth WC, Tuttle OF (1966) The alkali feldspar solvus in the system Na₂O–K₂O–Al₂O₃–SiO₂–H₂O. *Am Mineral* 51:1359–1373
- Ol'shanskii YI (1951) Composition of immiscible liquids in volcanic rocks. *Contrib Mineral Petrol* 80:201–218
- Orville PM (1963) Alkali ion exchange between vapor and feldspar phases. *Am J Sci* 261:201–237
- Powell R (1974) A comparison of some mixing models for crystalline silicate solid solutions. *Contrib Mineral Petrol* 46:265–274
- Powell R (1978) *Equilibrium thermodynamics in petrology*. Harper and Row, New York
- Powell R (1987) Darken's quadratic formalism and the thermodynamics of minerals. *Am Mineral* 72:1–11
- Powell R, Holland TJB (1988) An internally consistent dataset with uncertainties and correlations. 3. Applications to geobarometry, worked examples and a computer program. *J Metamorph Geol* 6:173–204
- Powell R, Holland TJB (1993) On the formulation of simple mixing models for complex phases. *Am Mineral* 78:1174–1180
- Powell R, Holland TJB, Worley B (1998) Calculating phase diagrams with THERMOCALC: methods and examples. *J Metamorph Geol* 16:577–588
- Prausnitz JM, Lichtenthaler RN, de Azevedo EG (1986) *Molecular thermodynamics of fluid-phase equilibria*, 2nd edn. Prentice-Hall, Englewood Cliffs
- Saxena SK, Fei Y (1988) Fluid mixtures in the C–H–O system at high pressure and temperature. *Geochim Cosmochim Acta* 52:505–512
- Shi P, Saxena SK (1992) Thermodynamic modeling of the C–H–O–S fluid system. *Am Mineral* 77:1038–1049
- Takenouchi S, Kennedy GC (1964) The binary system H₂O–CO₂ at high temperatures and pressures. *Am J Sci* 262:1055–1074
- Thompson JB Jr, Waldbaum DR (1968a) Mixing properties of sanidine crystalline solutions. I. Calculations based on ion-exchange data. *Am Mineral* 53:1965–1999
- Thompson JB Jr, Waldbaum DR (1968b) Analysis of the two-phase region halite-sylvite in the system NaCl–KCl. *Geochim Cosmochim Acta* 33:671–690
- Thompson JB, Waldbaum DR (1969) Mixing properties of sanidine crystalline solutions. III: calculations based on two phase data. *Am Mineral* 54:811–838
- Todheide K, Franck EV (1963) Das Zweiphasengebiet und die kritische Kurve im System Kohlendioxid–Wasser bis zu Drucken von 3500 bar. *Zeitsch Phys Chem* 37:387–401
- van Laar JJ (1906) *Sechs Vorträge über das Thermodynamischer Potential*. Vieweg, Brunswick
- White RW, Powell R, Holland TJB (2001) Calculation of partial melting equilibria in the system Na₂O–CaO–K₂O–FeO–MgO–Al₂O₃–SiO₂–H₂O (NCKFMASH). *J Metamorph Geol* 19:139–153
- Wood BJ, Banno S (1973) Garnet-orthopyroxene and orthopyroxene-clinopyroxene relationships in simple and complex systems. *Contrib Mineral Petrol* 42:109–124